Materials
Views
www.MaterialsViews.com

ADVANCED
MATERIALS
www.advmat.de

COMMUNICATION

# PS-*b*-P3HT Copolymers as P3HT/PCBM Interfacial Compatibilizers for High Efficiency Photovoltaics

*Zhenzhong Sun, Kai Xiao,* Jong Kahk Keum, Xiang Yu, Kunlun Hong, Jim Browning, Ilia N. Ivanov, Jihua Chen, Jose Alonzo, Dawen Li,* Bobby G. Sumpter, Edward A. Payzant, Christopher M. Rouleau, and David B. Geohegan*

Polymer bulk heterojunction (BHJ) solar cells have drawn worldwide attention due to their potential as a green, flexible, and low-cost renewable energy source.[1,2] A blend of regioregular poly(3-hexylthiophene) (rr-P3HT) and [6,6]-phenyl-$C_{61}$-butyric acid methyl ester (PCBM) is one of the most widely used material systems up to now. The phase separation of this binary system and the consequent effects on photovoltaic performance has been examined extensively in a number of studies. BHJ solar cells based on a P3HT/PCBM system typically give efficiencies in the range of 3-5%,[3,4] Despite continuous improvement in efficiency, P3HT/PCBM based BHJ solar cells still suffer from two major drawbacks: a poorly controlled electron donor (D) P3HT/acceptor (A) PCBM domain size distribution and inherent thermal instability on morphology.[5] Note that the phase separation in the blend is kinetically determined by processing conditions, and further coarsening of each individual phase domain is inevitable as heat is generated during continuous device operation.[6] Consequently, the resulting domain size can eventually become much larger than the exciton diffusion length (less than 10 nm), and device performance inevitably degrades.[7,8] Accordingly, morphology control and formation of a nanoscale interpenetrating network of P3HT/PCBM via phase separation tuning is one of the critical issues to achieve high-efficiency polymer BHJ solar cells with improved stability.

Z. Sun, Prof. D. Li
Department of Electrical and Computer Engineering
Center for Materials Information Technology
University of Alabama
Tuscaloosa, AL 35487, USA
E-mail: dawenl@eng.ua.edu
Dr. K. Xiao, Dr. X. Yu, Dr. K. Hong, Dr. I. N. Ivanov, Dr. J. Chen,
Dr. B. G, Sumpter, Dr. E. A. Payzant, Dr. C. M. Rouleau,
Dr. D. B. Geohegan
Center for Nanophase Materials Sciences
Oak Ridge National Laboratory
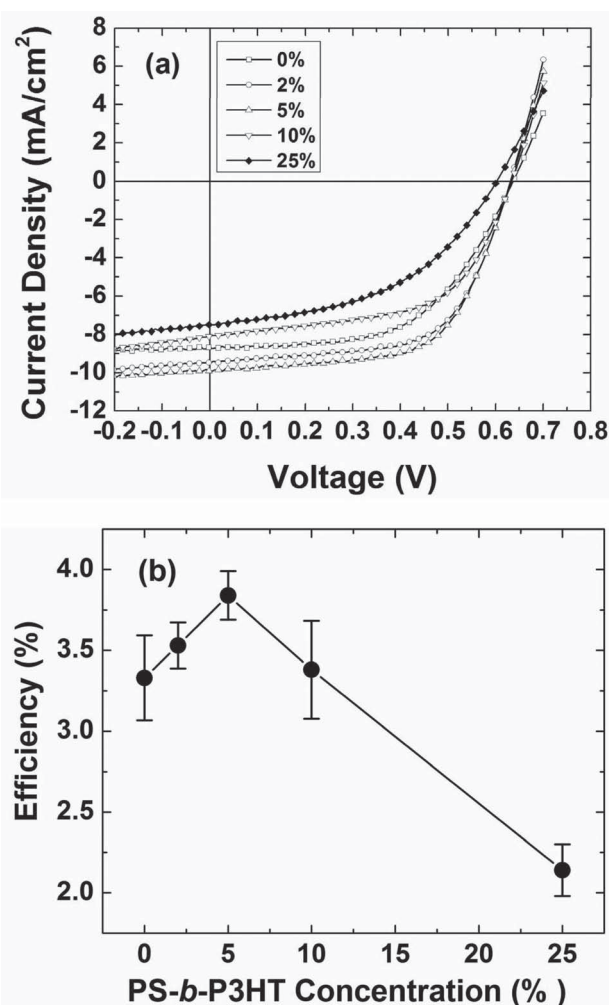Oak Ridge, TN 37831, USA
E-mail: xiaok@ornl.gov
Dr. J. K. Keum, Dr. J. Browning, Dr. J. Alonzo
Neutron Scattering Science Division
Oak Ridge National Laboratory
Oak Ridge, TN 37831, USA
Dr. B. G. Sumpter
Computer Science & Mathematics Division
Oak Ridge National Laboratory
Oak Ridge, TN 37831, USA

In an effort to improve the power-conversion efficiency (PCE), various studies have been performed to control the donor-acceptor morphology.[4,9–11] Recently, block copolymers comprised of P3HT as a block component have found applications as compatibilizers in P3HT/PCBM blends. It is well known that a proper compatibilizer can reduce interfacial tension and suppress coalescence, thereby limiting D/A domain sizes and improving morphological stability in the blend system.[12] Yang *et al.*, for example, synthesized rod-coil block copolymers, and added them to P3HT/PCBM blends as a surfactant, resulting in a substantial improvement in efficiency. Thelakkat *et al.*[14] reported an enhancement of phase separation by applying the donor-acceptor block copolymer, P3HT-*b*-poly(perylene bisimide acrylate) as a compatibilizer. Sary *et al.*[15] has reported that P3HT-*b*-P4VP can make an improvement for thermal stability as well as increase internal quantum efficiencies. To address macrophase separation in the P3HT/PCBM active layer, more recent studies by Sivula *et al.*[16] and Lee *et al.*[17] have demonstrated a suppression of large phase separation during thermal annealing. However, the short-circuit current densities of these devices are lower than those initially exhibited by the reference solar cells i.e., without any additional block copolymer. The reduction in short-circuit current density was attributed to the presence of large insulating groups or saturated hydrocarbon backbones in these block copolymers that ultimately hinder charge separation and transport.[16] Therefore, a critical component in the execution of a compatibilizer approach is the choice of diblock copolymer architecture, one that ensures that charge transport in the blend is not impeded by the presence of the compatibilizer while still maintaining the advantages of morphology optimization, and thermal stabilization imparted from the block copolymer. To our knowledge, although device performance has been routinely reported with the addition of copolymer compatibilizers, more detailed and systematic analyses of the buried morphology variation by incorporation of compatibilizers are very limited in thin films for solar energy conversions. There is a need to develop a fundamental understanding of the effect of block copolymer compatibilizer on the miscibility and crystallinity of the donor and acceptor components within these films with the ultimate goal of a detailed understanding and the ability to control molecular ordering, morphology, and phase-separation.

In this study, we utilize the diblock copolymer, polystyrene-*block*-poly(3-hexylthiophene) (PS-*b*-P3HT), to control P3HT/PCBM blend morphology, and enhance the P3HT crystallinity, thereby effectively improve power-conversion efficiency. A combination of semiconducting regioregular P3HT block and

non-conjugated flexible PS block has been shown to generate various highly organized structures (around 10–12 nm at the scale of exciton diffusion length). The well-organized nanostructures result from the interplay between self-assembly (e.g. π–π stacking) and phase separation.[18,19] In particular, the well-defined PS-*b*-P3HT diblock copolymer containing 85 wt% P3HT has demonstrated much higher carrier mobility than pristine P3HT, due to the increased crystallinity.[19] The efficient charge transport in PS-*b*-P3HT diblock copolymer motivates us to incorporate this copolymer as a compatibilizer in a P3HT/PCBM blend. In addition, significant interactions between two blocks of PS-*b*-P3HT diblock copolymer and the P3HT/PCBM blend are expected because of the similarities in the chemical structure of the PS-*b*-P3HT diblock copolymer to the P3HT/PCBM blend. The anticipated favorable molecule-block interactions could facilitate morphology optimization and stabilization against the destructive thermal phase segregation. In this work the effects of different amounts of PS-*b*-P3HT block copolymer on P3HT crystallinity and stacking orientation, morphology of P3HT/PCBM blend, and block copolymer - P3HT/PCBM interaction from all-electron density function theory (DFT) simulation, were studied and correlated to solar cell performance. By adding 5 wt% PS-*b*-P3HT diblock copolymer to the P3HT/PCBM blend, the crystallinity of P3HT is enhanced, which facilitates hole transport, resulting in an improved charge transport balance. We also found that the PS-*b*-P3HT compatibilizer was able to effectively modify P3HT/PCBM phase separation, leading to a desirable nanoscale interpenetrating D/A network for efficient exciton dissociation. Neutron reflectivity experiments show that the addition of the block copolymer has a positive effect on phase separation and can be used in controlling the vertical morphology of the active layer, especially the PCBM accumulation near the substrate interface and amount of PCBM in the middle layer. Enhanced hole transport and optimized morphology work together, resulting in an increased short-circuit current density and fill factor for improved power-conversion efficiency up to 4.1%.
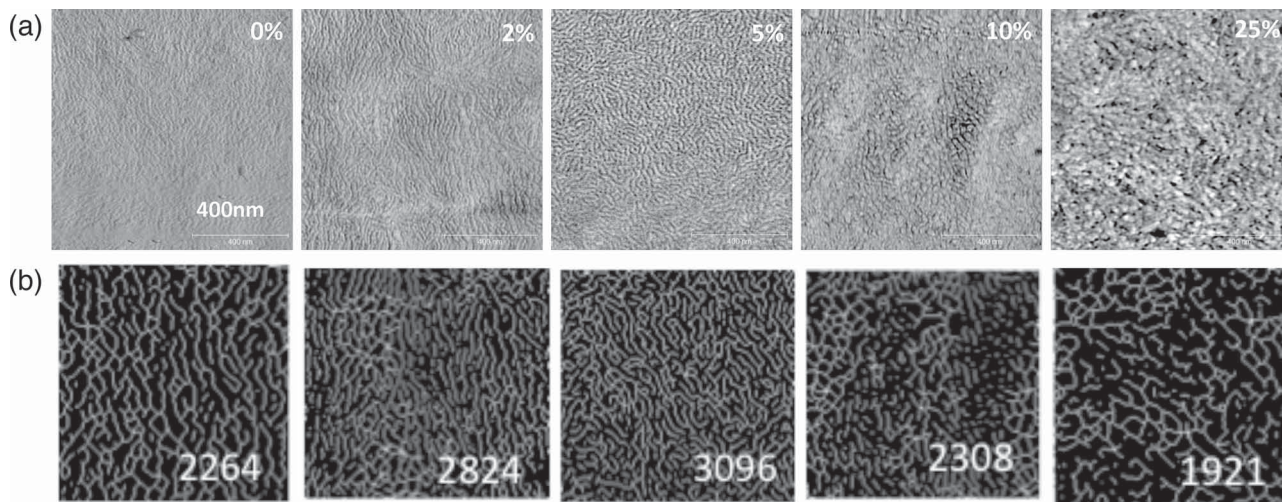
**Figure 1**a compares the current density versus voltage (*J*–*V*) curves of P3HT/PCBM solar cells for different amounts of PS-*b*-P3HT block copolymer. The photovoltaic parameters, such as the short-circuit current density ($J_{SC}$), open-circuit voltage ($V_{OC}$), fill factor (FF), and power-conversion efficiency (PCE) are summarized in Table S1. The performance of the photovoltaic cells was found to depend significantly on the amount of PS-*b*-P3HT copolymer. Without adding any PS-*b*-P3HT copolymer, a PCE of 3.3% was obtained. Upon adding 2% amount of PS-*b*-P3HT copolymer, the efficiency increased to 3.8%. The best performance was achieved when 5 wt% PS-*b*-P3HT polymer was added, whereby $V_{OC}$ = 0.63 V, $J_{SC}$ = 9.86 mA/cm², FF = 0.62, and PCE of 4.1% were achieved. Further increasing the content of compatibilizer, however, results in a decrease of efficiency. As shown in Table S1, PCE reflects the dependence of the short-circuit current density and fill factor on the amount of diblock copolymer, i.e., PCE is determined by $J_{SC}$ and FF. The incorporation of PS-*b*-P3HT copolymer does not significantly affect open-circuit voltage. As is well known, the energy level difference between the LUMO of PCBM and the HOMO of P3HT is one important factor that determines the open-circuit voltage. Obviously, the small amounts of PS-*b*-P3HT



**Figure 1.** (a) *J*–*V* characteristics of BHJ polymer solar cells, (b) power-conversion efficiency (Error bar from standard deviation was based on 6-10 device samples).

copolymer do not strongly affect the HOMO energy level of P3HT and LUMO level of PCBM (detailed analysis and DFT calculation can be found in supporting information). As shown in Figure 1, the PS-*b*-P3HT copolymer is an effective compatibilizer to enhance the efficiency of BHJ solar cells when 5% was added to P3HT/PCBM blend. Further addition of PS-*b*-P3HT copolymer likely introduces too much low molecular weight P3HT and insulating PS component in the P3HT/PCBM blend, thereby degrading the device performance.

The active layer morphology is critical for BHJ polymer solar cell performance. Here, we studied the surface morphology of P3HT/PCBM blend with addition of block copolymer compatibilizer using atom force microscopy (AFM), and investigated the buried morphology using the advanced scattering technique grazing-incidence X-ray scattering (GIXS) in combination with neutron reflectometry. The information about the structure and crystallinity of the film from GIXS along with the composition profile normal to the film surface from neutron reflectometry as well as the surface topography from AFM allow us to reconstruct the film morphology.
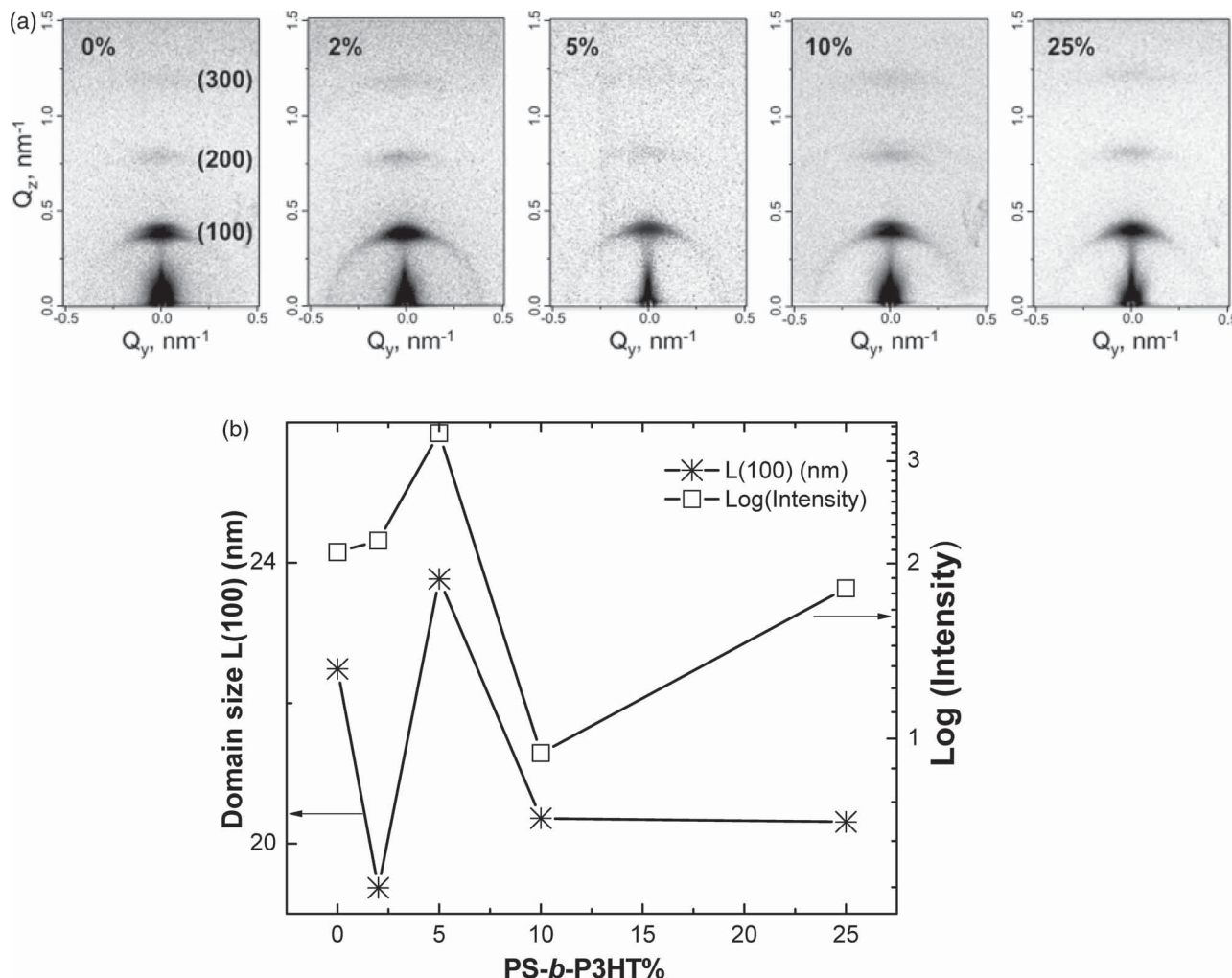
**Figure 2.** (a) AFM phase images of P3HT/PCBM thin film with different PS-*b*-P3HT diblock copolymer concentrations. (b) The features in the mid-frequency range after Fourier transform for 5% sample correlates well with establishing better ordering of the polymer composite illustrated through skeletonization of bright phase areas of original AFM phase image down to a single pixel. The skeletized images allow assessment of inter-connection network of phases as well as their surface area (estimated from the white pixel count). The samples with 5% of PS-*b*-P3HT showed the longest network of phases with the largest surface area.

An uniform morphology with an interpenetrating network of P3HT and PCBM nanoscale domains is desirable for excitons to be able to diffuse to the heterojunction and dissociate at the D/A interface.[20] As shown in **Figure 2**, such uniform morphology with interpenetrating nanoscale P3HT and PCBM domains has been achieved at 5% concentration of PS-*b*-P3HT diblock copolymer, which corresponds to the highest efficiency achieved in this study. Further increases in the concentration of PS-*b*-P3HT copolymer beyond 5%, resulted in large sphere-like aggregates on the surface, which are likely due to PS-*b*-P3HT diblock copolymer self-assembly. The strong interaction between PS block and PCBM molecules (shown in computer simulation) could make PCBM accumulate within PS block, causing a large aggregation of PCBM clusters. Fourier transform magnitudes of original AFM phase images for various fraction of PS-*b*-P3HT are plotted in Figure S1. The features in the mid-frequency range for 5% sample correlates well with establishing better ordering of the polymer composite illustrated through skeletonization of bright phase areas of original AFM phase image down to a single pixel, as shown in Figure 2 b. The skeletized images allow assessment of inter-connection network of phases as well as their surface area (estimated from the white pixel count). The samples with 5% of PS-*b*-P3HT showed the longest network of phases with the largest surface area.

**Figure 3**a displays the two-dimensional (2D) GIXS patterns of P3HT/PCBM thin films with the various amounts of PS-*b*-P3HT copolymer. The (100), (200), and (300) diffraction peaks are strong in the out-of-plane direction. This means that the P3HT/PCBM blend films have a well-organized structure in which most of the *a*-axis of P3HT domain is oriented along the direction perpendicular to the substrate. From the scattering pattern of (100), we extracted a *d*-spacing of 1.59 nm, which is consistent with data reported elsewhere.[21] The P3HT crystallite

size estimated using the Scherrer equation and the area of the P3HT (100) peak representing the relative crystallinity of P3HT in the films are plotted as a function of the fraction of PS-*b*-P3HT copolymer in the blend (Figure 3b). There is no significant difference in the *d*-spacing of (100) reflection regardless of the fraction of copolymer compatibilizer. However, the normalized area under the (100) peak and the peak sharpness indicates a transformation in crystallinity and crystallite domain size with the addition of compatiblizers. The sample with 5% of PS-*b*-P3HT presents the highest peak intensity (crystallinity) and largest domain size (Figure 3b). This indicates that adding the diblock copolymer into a P3HT/PCBM blend is an effective strategy to induce well organized crystalline P3HT domains in the blend. Another important influence of the added compatibilizer is the variation in the degree of orientation of P3HT domain. The azimuthal distribution of (100) reflection intensity is shown in Figure S2. Indeed, the comparison of azimuthal angular breadth of the P3HT (100) peaks did not show clear difference between sample. However, the degree of crystal orientation calculated based on the azimuthal intensity distribution of (100) reflection revealed a clear trend as shown in Figure S2 (c). It can be seen that the degree of crystal orientation increases with increasing diblock copolymer contents and remains unchanged above 5% copolymer content. The higher crystallinity and crystal orientation of P3HT can enhance hole transport in P3HT domain, leading to an improved charge transport balance between electrons and holes thereby increasing current density and fill factor.[22,23]
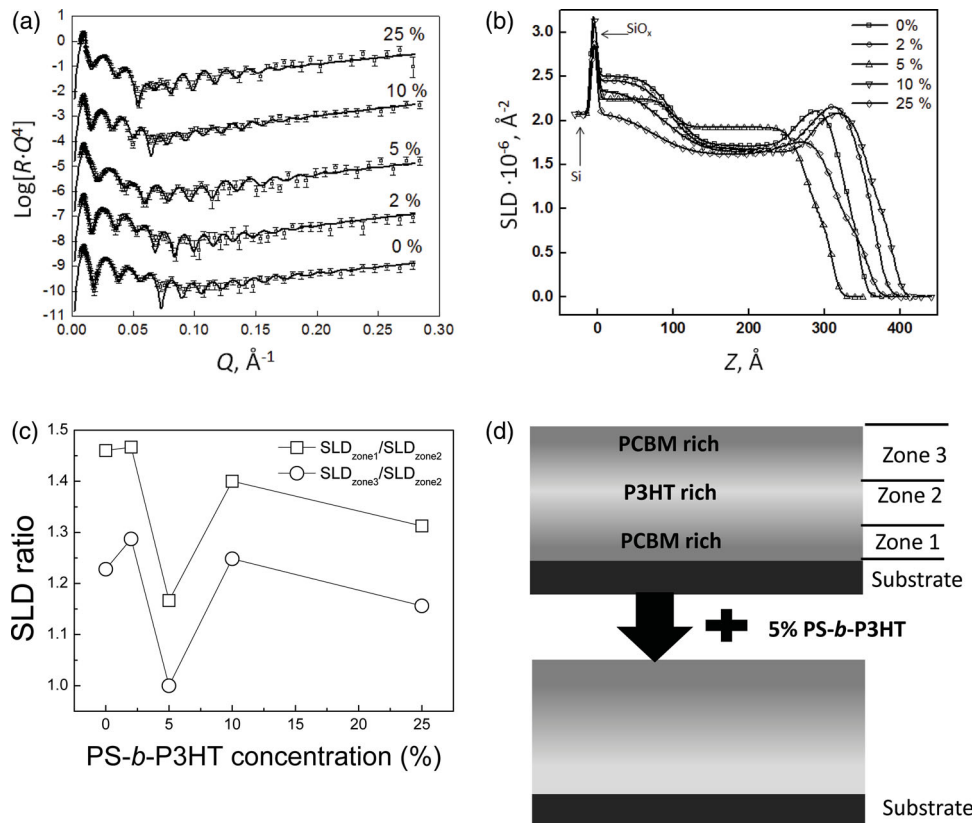
Neutron Reflectivity (NR) is very useful for profiling the phase and buried interfacial morphology of blend films in the direction normal to substrate.[24,25] Recently, NR has been successfully used to elucidate the vertical concentration profile of active layers in P3HT/PCBM solar cells due to the high natural contrast in scattering length density (SLD) existing between

**Figure 3.** (a) 2D GIXS patterns of the P3HT/PCBM films with the addition of 0, 2, 5, 10, and 25% of PS-*b*-P3HT block copolymer. $Q_z$ and $Q_y$ are the perpendicular and parallel wave vector transfer with respect to substrate surface. (b) The domain size and normalized peak intensity of (100) extracted from 1D GIXS measurement.

P3HT and PCBM.[26–28] **Figure 4**a shows the NR profiles of a series of spin-coated films with different PS-*b*-P3HT concentrations. The solid lines are the best fits to the data obtained using the models (SLD profiles) shown in Figure 4b. The NR calculation and data fit were based on a standard iterative formula using a series of layers to approximate the scattering length density profile and error function to account for rough interfaces.[29] The best fits for the films with 0, 2, 10 and 25% PS-*b*-P3HT were obtained using a three-layer model that consisted of a top layer near air/polymer interface, a middle layer around the center of film along the thickness direction, and a bottom layer near polymer/substrate. Whereas, the best fit for the NR data measured the film with 5% PS-*b*-P3HT was obtained using two-layer model consisting of top and bottom layers without distinct middle layer. We note that the thicknesses, *d*, obtained by NR were corroborated using ellipsometry. As shown in Figure 4b, the NR data of pristine P3HT/PCBM film shows that PCBM with high SLD are segregated and accumulated at both near the air/polymer and polymer/substrate interfaces leading to higher SLD, which is consistent with previously reported

results.[30] Adding PS-*b*-P3HT copolymer in different fractions, however, induced the changes in the SLD distribution in the films. In order to compare the phase homogeneity between films in more detail, the films were first subdivided into three equi-thickness zones depending on the distance from the substrate, i.e., zone 1 for $0 \leq z < d/3$, zone 2 for $d/3 \leq \zeta < 2d/3$ and zone 3 for $2d/3 \leq z \leq d$, then the SLD ratio between zones (i.e. for both zone 1/zone 2 and a zone 2/zone 3) were calculated, where the ratio can be used as a indication to determine relative phase homogeneity of the blends. For example, a ratio of 1 indicates homogeneous phase while the ratio deviates more from 1 as the phase becomes less homogeneous. With increasing the contents of compatibilizer up to 5%, the SLD ratio of zone 1/zone 2 and zone 2/zone 3 decrease close to 1, then increase with increasing compatibilizer contents above 5% (Figure 4c). The initial decreases in SLD ratio indicates that the amounts of PCBM near the substrate/film and the air/film interface decrease resulting in the increase in PCBM concentration in zone 2. One of the most interesting that can be found in Figure 4 is that the SLD profile of film with 5% compatibilizer is very
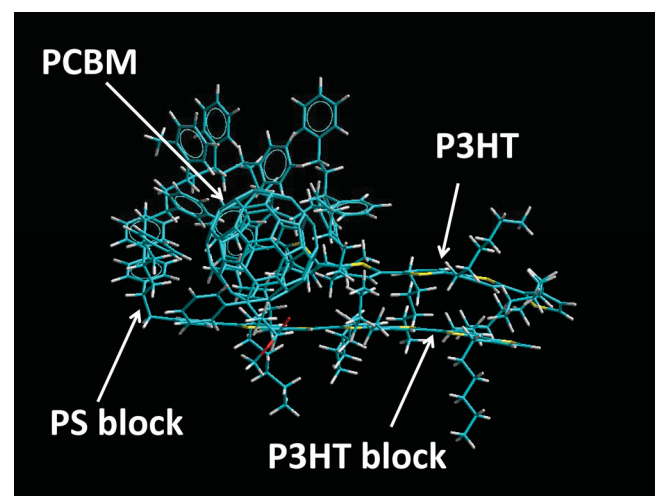
**Figure 4.** (a) Reflectivity (R) multiplied by perpendicular wave vector transfer ($Q_z$) to the fourth power ($RQ_z^4$) vs $Q_z$ for a silicon wafer with a thin film of P3HT/PCBM blend with various fraction of PS-*b*-P3HT polymer. The solid lines represent the best fits to the NR data of the thin films as described in the text while the markers represent the experiment data. In the data fit, mass balance was maintained. (b) SLD profile of the films as determined from the fitting. (c) The SLD ratio ($SLD_{zone1}/SLD_{zone\,2}$, $SLD_{zone\,3}/SLD_{zone\,2}$) vs fraction of PS-*b*-P3HT compatibilizers. (d) The schematic of the vertical SLD profile in thin film from the model fit.

different from others showing only two distinct layers. Also, the SLD ratio were the least among samples. Clearly the addition of 5% of PS-*b*-P3HT copolymer in P3HT/PCBM restricts the segregation of PCBM leading to a more homogeneous film. This can be correlated to the enhanced miscibility of the components, as indicated by the finding that the PS-*b*-P3HT copolymer forms a preferable orientation at the P3HT/PCBM interface and the enhanced effective interaction between P3HT and PCBM shown by DFT calculations in **Figure 5**. Although there is still an accumulation of PCBM near the substrate interface, the film with 5% compatibilizer is clearly more favorable than other films and exhibit the highest PCE. Moreover, the optical microscope images of the solar cells (Figure S3) show that the incorporated PS-*b*-P3HT copolymer also reduced the PCBM aggregation upon heating, resulting better in thermal stability.

All-electron density function theory (DFT) calculations were used to provide additional insight into the molecular interactions between the different oligomeric units (3HT, styrene) and PCBM, as well as to explore the structural arrangements of molecules that lead to the interactions. For these calculations the 6-31G∗ basis set and the local density approximation were used. The gas phase oligomer-PCBM and oligomer-oligomer interaction energies are computed by the difference in energy of the optimized polymer-PCBM pair and the individual components with corrections to basis set superposition error (BSSE) and deformation energy.[31,32] The interaction energies between

different components in the P3HT/PCBM/PS-*b*-P3HT blends are listed in Table S2. The interaction energy between PS and PCBM (3.52 kcal.mol$^{-1}$.monomer$^{-1}$) is larger than that of a



**Figure 5.** Configuration taken from a fully optimized structure of an oligomeric blend of P3HT/PCBM with a single copolymer chain of PS-*b*-P3HT. The molecular snapshot showing only one PCBM and P3HT, was obtained from a 100 picosecond molecular dynamics simulation of a small 1:1 PCBM/P3HT system (5 P3HT/5 PCBM) with a single PS-*b*-P3HT molecule added.

P3HT-PCBM pair (3.05 kcal.Mol$^{-1}$.monomer$^{-1}$), and the inter-action energy of a P3HT-PS pair (1.61 kcal.Mol$^{-1}$.monomer$^{-1}$) is substantially smaller than that of a P3HT-P3HT pair (2.95 kcal.Mol$^{-1}$.monomer$^{-1}$). Based on a purely enthalpic contribution, a copolymer of PS-*b*-P3HT can form a preferable orientation at the P3HT/PCBM interface, such that the P3HT block interacts directly with the P3HT domains of the P3HT/PCBM blend, and the PS block prefers interaction with the PCBM molecule. Indeed a semi-empirical model based on PM3[33] optimized structure (obtained after 100 picoseconds of molecular dynamics simulation at room temperature) shows that the copolymer acts like a plasticizer by diffusing to the PCBM/P3HT interface (see Figure 5). The PS-*b*-P3HT compatibilizer tends to promote the microphase segregation with the PCBMs moving toward the PS block and the P3HT and P3HT block forming regular stacks with a presumably improved "crystallinity", consistent with the GIXS and neutron reflectivity results.

In summary, we have demonstrated that a small amount of a PS-*b*-P3HT diblock copolymer could serve as a compatibilizer to effectively improve the power-conversion efficiency of P3HT/PCBM based photovoltaic cells. At optimal concentrations, the diblock copolymer was found to induce favorable active layer morphology with interpenetrating nanoscale domains, and the enhanced P3HT crystallinity and orientation facilitate hole transport within the active layer. Quantum density functional theory calculations suggest that the interaction between PS segments and PCBM is a major driving force to control phase separation in P3HT/PCBM blends, with the PCBM attracted to the PS block, and the P3HT stacking onto the P3HT block, which leads to improvements in long-range "crystallinity". NR results show that the addition of the PS-*b*-P3HT compatibilizer affects the PCBM segregation in the vertical direction, in which the PCBM accumulation near the substrate interface is reduced with a corresponding increase in the middle region of the active layer. The most homogeneous profile was obtained at the PS-*b*-P3HT concentration of 5 wt%, which we attribute to an increase in miscibility of P3HT and PCBM driven by the copolymer compatibilizer. Overall, the addition of diblock copolymers to control phase separation, crystallinity, and resultant favorable composition profile in vertical direction represents a promising way to enhance the photovoltaic properties of polymer bulk heterojunction solar cells. Similar improvements are observed on the thermal stability of these more crystalline, ordered structures. Systematic studies on the effects of PS-*b*-P3HT diblock copolymer on the thermal stability of P3HT/PCBM blend devices are underway.

## Experimental Section

P3HT (50 kDa) was commercially available from Rieke Metal Inc, and PCBM was purchased from NanoC. These chemicals were used directly without further purification. Poly(3,4-ethylenedioxy thiophene): poly (styrene sulfonate) (PEDOT:PSS) purchased from HC Stark was passed through a 0.45 m filter and spin-coated on the ITO glass substrates. The PS-*b*-P3HT copolymer was synthesized as described in reference.[19] The PS-*b*-P3HT (15:85 wt%) copolymer used in this work had a weight-average molecular weight (MW) of 13300 and a polydispersity of 1.32. Films for NR were spin-coated at 1500 rpm for 40 s onto 2" wafers.

The photovoltaic cells were fabricated using the following procedure: A blend solution was prepared by dissolving P3HT/PCBM (1:0.7 wt) in 1,2-dichlorobenzene (DCB) at a concentration of 20 mg/ml, and the PS-*b*-P3HT copolymer was added to the P3HT/PCBM blend at different ratios of 2, 5, 10, 25 wt%. The P3HT/PCBM/PS-*b*-P3HT blend solution was heated on hotplate at 60 °C overnight before device fabrication. ITO glass substrates were cleaned by soap and ultrasonic agitation in DI water, acetone and isopropyl alcohol (IPA). The cleaned substrates were treated with UV Ozone for 20 minutes. Filtered PEDOT:PSS was spin-coated on ITO glass at 5000 rpm for 40 s and dried at 140 C for 10 minutes in air. The mixed P3HT/PCBM/PS-*b*-P3HT solution was spin-coated on the top of PEDOT:PSS layer at a spin speed of 900 rpm for 40 s. The resulting film thickness is about 80 nm. After spin-coating the films were annealed at 140 C for 20 minutes in a vacuum oven. Finally the device fabrication was completed by thermal evaporation of the top metal cathode (15 nm Ca and 85 nm Al) through a shadow mask. Current-voltage (I-V) characterization of the polymer photovoltaic cells was conducted using a computer-controlled measurement unit from Newport under the illumination of AM1.5G, 100 mW/cm$^2$.

## Supporting Information

Supporting Information is available from the Wiley Online Library or from the author.

## Acknowledgements

[1] N. S. Sariciftci, L. Smilowitz, A. J. Heeger, F. Wudl, *Science* **1992**, *258*, 1474.

[2] M. Sommer, A. S. Lang, M. Thelakkat, *Angew. Chem. Int. Ed.* **2008**, *47*, 7901.

[3] M. T. Dang, L. Hirsch, G. Wantz, *Adv. Mater.* **2011**, *23*, 3597.

[4] G. Li, Y. Yao, H. Yang, V. Shrotriya, G. Yang, Y. Yang, *Adv. Funct. Mater.* **2007**, *17*, 1636.

[5] J. H. Tsai, Y. C. Lai, T. Higashihara, C. J. Lin, M. Ueda, W. C. Chen, *Macromolecules.* **2010**, *43*, 6085.

[6] J. J. M. Halls, K. Pichler, R. H. Friend, S. C. Moratti, A. B. Holmes, *Appl. Phys. Lett.* **1996**, *68*, 3120.

[7] R. H. Friend, G. J. Denton, J. J. M. Halls, N. T. Harrison, A. B. Holmes, A. Kohler, A. Lux, S. C. Moratti, K. Pichler, N. Tessler, K. Towns, *Synth. Met.* **1997**, *84*, 463.

[8] D. E. Markov, C. Tanase, P. W. M. Blom, J. Wildeman, *Phy. Rev. B.* **2005**, *72*, 045217

[9] M. Brinkmann, F. Chandezon, R. B. Pansu, C. Julien-Rabant, *Adv. Funct. Mater.* **2009**, *19*, 2759.

[10] J. K. Lee, W. L. Ma, C. J. Brabec, J. Yuen, J. S. Moon, J. Y. Kim, K. Lee, G. C. Bazan, A. J. Heeger, *J. Am. Chem. Soc.* **2008**, *130*, 3619.

[11] G. Li, V. Shrotriya, Y. Yao, Y. Yang, *J. Appl. Phys.* **2005**, *98*, 043704.

[12] J. A. Galloway, H. K. Jeon, J. R. Bell, C. W. Macosko, *Polymer.* **2005**, *46*, 183.

[13] C. Yang, J. K. Lee, A. J. Heeger, F. Wudl, *J. Mater. Chem.* **2009**, *19*, 5416.

[14] M. Sommer, S. Huttner, U. Steiner, M. Thelakkat, *Appl. Phys. Lett.* **2009**, *95*, 183308.

[15] N. Sary, F. Richard, C. Brochon, N. Leclerc, P. Leveque, J. N. Audinot, S. Berson, T. Heiser, G. Hadziioannou, R. Mezzenga, *Adv. Mater.* **2010**, *22*, 763.

[16] K. Sivula, Z. T. Ball, N. Watanabe, J. M. J. Frechet, *Adv. Mater.* **2006**, *18*, 206.

[17] J. U. Lee, J. W. Jung, T. Emrick, T. P. Russell, W. H. Jo, *Nanotechnology* **2010**, *21*, 105201.

[18] J. S. Liu, E. Sheina, T. Kowalewski, R. D. McCullough, *Angew. Chem. Int. Ed.* **2002**, *41*, 329.

[19] K. Xiao, X. Yu, J. Chen, N. V. Lavrik, K. Hong, B. G. Sumpter, D. B. Geohegan, *ACS Nano* **2011**, *5*, 3559.

[20] W. L. Ma, C. Y. Yang, X. Gong, K. Lee, A. J. Heeger, *Adv. Funct. Mater.* **2005**, *15*, 1617.

[21] M. Y. Chiu, U. S. Jeng, M. S. Su, K. H. Wei, *Macromolecules* **2010**, *43*, 428.

[22] A. J. Moule, K. Meerholz, *Adv. Mater.* **2008**, *20*, 240.

[23] J. Peet, A. J. Heeger, G. C. Bazan, *Acc. Chem. Res.* **2009**, *42*, 1700.

[24] Y. S. Chung, N. Shin, J. Kang, Y. Jo, V. M. Prabhu, S. K. Satija, R. J. Kline, D. M. DeLongchamp, M. F. Toney, M. A. Loth, B. Purushothaman, J. E. Anthony, D. Y. Yoon, *J. Am. Chem. Soc.* **2011**, *133*, 412.

[25] D. A. Chen, A. Nakahara, D. G. Wei, D. Nordlund, T. P. Russell, *Nano Lett.* **2011**, *11*, 561.

[26] K. H. Lee, P. E. Schwenn, A. R. G. Smith, H. Cavaye, P. E. Shaw, M. James, K. B. Krueger, I. R. Gentle, P. Meredith, P. L. Burn, *Adv. Mater.* **2011**, *23*, 766.

[27] A. J. Parnell, A. D. F. Dunbar, A. J. Pearson, P. A. Staniec, A. J. C. Dennison, H. Hamamatsu, M. W. A. Skoda, D. G. Lidzey, R. A. L. Jones, *Adv. Mater.* **2010**, *22*, 2444.

[28] D. M. Huang, S. A. Mauger, S. Friedrich, S. J. George, D. Dumitriu-LaGrange, S. Yoon, A. J. Moulé, *Adv. Funct. Mater.* **2011**, *21*, 1657.

[29] T. P. Russell, *Mater. Sci. Rep.* **1990**, *5*, 171.

[30] J. W. Kiel, B. J. Kirby, C. F. Majkrzak, B. B. Maranville, M. E. Mackay, *Soft Matter* **2010**, *6*, 641.

[31] R. A. Kendall, E. Apra, D. E. Bernholdt, E. J. Bylaska, M. Dupuis, G. I. Fann, R. J. Harrison, J. L. Ju, J. A. Nichols, J. Nieplocha, T. P. Straatsma, T. L. Windus, A. T. Wong, *Comput. Phys. Commun.* **2000**, *128*, 260.

[32] D. Linton, P. Driva, B. Sumpter, I. Ivanov, D. Geohegan, C. Feigerle, M. D. Dadmun, *Soft Matter* **2010**, *6*, 2801.

[33] G. B. Rocha, R. O. Freire, A. M. Simas, J. J. P. Stewart, *J. Comput. Chem.* **2006**, *27*, 1101.